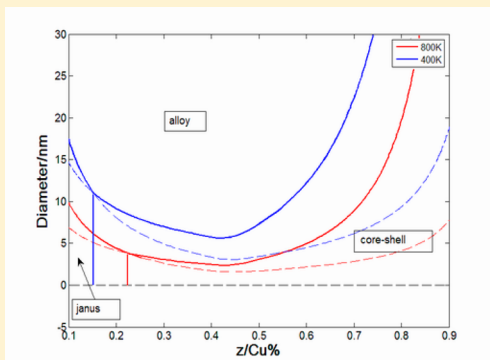


Modeling the Phase Stability of Janus, Core–Shell, and Alloyed Ag–Cu and Ag–Au Nanoparticles

Hongcheng Peng,[†] Weihong Qi,^{*,†,‡,§} Siqi Li,[†] and Wenhui Ji[†]

[†]School of Materials Science and Engineering, [‡]Institute for Materials Microstructure, and [§]Key Laboratory of Non-ferrous Materials Science and Engineering (Ministry of Education), Central South University, Changsha 410083, People's Republic of China

ABSTRACT: On the basis of the Gibbs free energy (GFE) model of Janus, core–shell, and alloyed structures of Ag–Cu and Ag–Au nanoparticles, the structural stability and size-composition phase diagram are obtained. For phase segregated structure, small size and low temperature are more beneficial at fixed composition. If the temperature is fixed, the segregated phase is favored at small size and low composition. The lowest critical size to phase segregation is 6 nm for Ag–Cu NPs and 4.5 nm for Ag–Au NPs at 400 K and Ag atom fraction of approximately 50%, and raising the temperature reduces the critical size. For Ag–Cu phase diagram, it is found that the core size is dominated by the transformation between Janus and core–shell structure. When the core is sufficient large, the Ag–Cu NPs will keep the core–shell structure. As the core size gets smaller, the core location will be moved from center to off-center until it forms quasi-Janus or Janus NPs. However, for the Ag–Au phase diagram, there is no Janus structure at large scale of composition.



1. INTRODUCTION

Bimetallic nanoparticles (NPs) have drawn increasing attention because of their fascinating physical and chemical properties, such as catalytic, optical, and magnetic properties, which are different from those of the corresponding bulk state, which may have numerous practical applications. The bimetallic NPs have drawn a lot of attention because their properties depend on size, structure, composition, and chemical ordering.^{1–3} Bimetallic NPs can present various chemical orderings, ranging from an alloyed to a segregated state.¹ A segregated state can be classified as core–shell and layered segregated. The latter has been named “Janus” NPs, which is the name of an ancient Roman God who has two faces oppositely. The degree of segregation between alloyed and atomic ordering in nanoparticles depends on the following factors: bond strength of homogeneous and heterogeneous atoms, surface energies of bulk elements, atomic sizes, strength of binding to surface ligands, etc.¹

Janus NPs have been one of the most interesting research objects, due to their asymmetric structures and totally different properties of “two faces” elements (Figures 1 and 2). For instance, Langlois et al.⁴ achieved the transition from Cu–Ag core–shell structure to Janus by annealing method. They also used density functional theory (DFT) calculations and molecular dynamics (MD) simulations to reproduce the transition process. Logsdail et al.⁵ predicted the optical properties of core–shell and Janus Au_{0.5}Ag_{0.5} NPs with a fixed overall radius of 2.5 nm. Parsina et al.⁶ compared Ag–Co core–shell and Janus-like structures by MD simulation using a semiempirical many-body potential. Their results showed that “Janus-like” structures naturally evolve to core–shell ones for

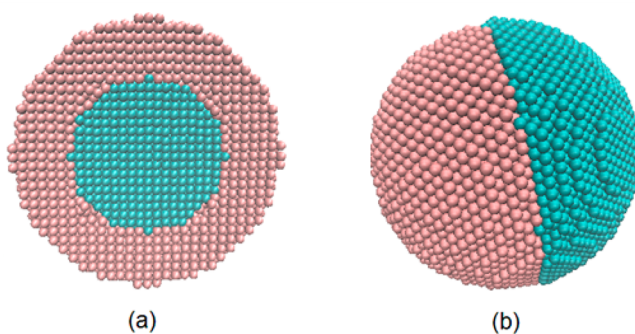


Figure 1. Cross-sectional view of the bimetallic core–shell (a) and Janus (b) NPs, respectively.

cobalt concentration of less than 40–45% at medium size. Song et al.⁷ synthesized Ag–Au Janus NPs with an average diameter of 5.36 ± 0.85 nm by interfacial galvanic exchange reaction. Xu et al.⁸ synthesized Co–Au core–shell and Janus structures in direct gas-phase method with different experimental conditions.

In our previous works, we focused on the thermodynamic stability of pure metal NPs,^{9,10} and bimetallic nanoalloy.¹¹ In this work, we aim at adapting our previous model into a bimetallic segregated system, and predicting the size-, composition-, and temperature-dependent structural stability of alloyed, core–shell, and Janus NPs. As far as we know, there is no reported work considering all of these factors together.

Received: October 25, 2014

Revised: January 3, 2015

Published: January 20, 2015



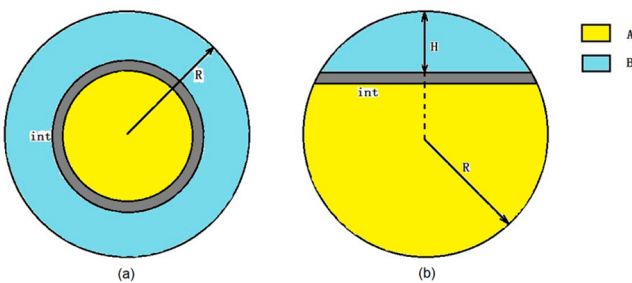


Figure 2. Schematic depiction of the core–shell (a) and Janus (b) NPs with three regions: region A, region B, and the interface.

We choose the Ag–Cu and Ag–Au systems as a model system to predict the structure stability. The Ag–Cu NPs have a relatively high size mismatch ($r_{\text{Ag}}/r_{\text{Cu}} = 1.13$), and hence the Ag–Cu system has an interior strain that cannot be neglected. Bochicchio et al.¹² studied the strain originating from size mismatch of Ag–Cu NPs and found that the strain relaxation is the driving force affecting the lowest energy configuration. In addition, Ag–Cu NPs have a positive formation enthalpy at bulk state (0.1111 eV/atom for Ag–Cu).¹³ Thus, the two elements are immiscible in bulk scale; it is more likely to form phase segregated structure for Ag–Cu at nanoscale. Meanwhile, the surface energies of Cu are obviously higher than that of Ag (0.707 eV/atom for Cu (111) plane, and 0.553 eV/atom for Ag (111) plane),¹³ so that Ag is more likely to stay at the surface leading to surface segregation.⁸ On the contrary, Ag–Au has a similar lattice constant ($r_{\text{Ag}} = 1.45 \text{ \AA}$, $r_{\text{Au}} = 1.44 \text{ \AA}$) and a negative formation enthalpy (−0.0672 eV/atom for Ag–Au).¹³ So the Ag–Au system is more likely to form alloyed structure in nanoscale. This Article is organized as follows: the model details are given in section 2, the calculation results and discussion are presented in section 3, and the conclusions are made in section 4.

2. MODEL

According to the basic thermodynamics theory, the Helmholtz free energy (HFE) is the sum of the cohesive energy and vibrational energy. For the phase segregation model, it should include one energy of the interface region. So, the HFE of Janus and core–shell NPs can be written as

$$\begin{cases} F_j = x_A F_A + x_B F_B + E_{\text{int}} \\ F_M = N E_p^M + N(E_{\text{vib}}^M - T S_{\text{vib}}^M) \end{cases} \quad (1)$$

where the subscript M denotes element A or B. x_A and x_B are atom number ratios of A and B, respectively. E_p is the cohesive energy per atom of the NPs, following the relationship with one of the bulk state E_b :¹⁴

$$E_p = E_b \left(1 - \frac{3\alpha d}{D}\right)$$

where E_b is the cohesive energy of bulk materials, d is the atomic diameter, and D is the diameter of NPs. α is the shape factor,¹⁵ which is the surface area ratio between nonspherical and spherical morphology of identical volume. For spherical NPs, $\alpha = 1$, and for regular tetrahedral NPs, $\alpha = 1.49$. In this Article, we only consider the spherical NPs; thus $E_p = E_b(1 - (3d/D))$.

E_{vib} and S_{vib} in eq 1 represent the vibrational energy and vibrational entropy, respectively. According to the Debye model,^{16,17} the two quantities can be expressed as

$$\begin{cases} E_{\text{vib}} = 3k_B T B\left(\frac{\Theta}{T}\right) + E_0 \\ S_{\text{vib}} = 4k_B \left[B\left(\frac{\Theta}{T}\right) - \frac{3}{4} \ln(1 - e^{-\Theta/T}) \right] \end{cases} \quad (2)$$

where k_B and Θ are Boltzmann constant and Debye temperature^{18,19} respectively. $E_0 = (9k_B\Theta)/8$ is the zero-point vibrational energy, which is usually ignored. $B(\Theta/T) = 3(T/\Theta)^3 \int_0^{\Theta/T} ((x^3)/(e^x - 1)) dx$ is the Debye function.

Because of the surface effect, the vibrational energy and vibrational entropy of NPs vary with the change of particle size. Sun et al.^{20,21} reported the lattice vibrational frequency (ω) of surface atoms and that of bulk atoms, and the relationship of the vibrational amplitude (χ) between surface atoms and bulk ones:

$$\frac{\omega_s}{\omega_b} = \frac{z_s}{z_b} C_z^{-(m/2+1)}, \quad \frac{\chi_s}{\chi_b} = \left(\frac{z_b}{z_s}\right)^{1/2} C_z^{m/2+1}$$

The subscripts s and b denote the surface and the bulk atoms, respectively. Z_s and Z_b are the coordination numbers of surface and bulk atoms. $C_z = 2/\{1 + \exp[(12 - z)/8z]\}$ is the bond contraction coefficient (z refers to the coordination number). According to Sun's theory,¹⁹ the value of ω_s/ω_b could be 0.41 and χ_s/χ_b could be 1.43.

The vibration energy is proportional to the square of its amplitude. Thus, the vibrational energy of surface atoms (E_{vib}^s) can be written as

$$E_{\text{vib}}^s = \left(\frac{\chi_s}{\chi_b}\right)^2 E_{\text{vib}} = 2E_{\text{vib}}$$

If the vibrational frequency of an atom varies from ω_b to ω_s , the vibrational entropy's change is $\Delta S_{\text{vib}} = 3k_B \ln(\omega_b/\omega_s)$. Thus, the vibrational entropy of surface atoms (E_{vib}^s) can be written as

$$\begin{aligned} S_{\text{vib}}^s &= S_{\text{vib}} + \Delta S_{\text{vib}} = 4k_B \left[B\left(\frac{\Theta}{T}\right) - \frac{3}{4} \ln(1 - e^{-\Theta/T}) \right] \\ &\quad + 3k_B \ln \frac{\omega_b}{\omega_s} \\ &= 4k_B \left[B\left(\frac{\Theta}{T}\right) - \frac{3}{4} \ln(1 - e^{-\Theta/T}) \right] + 2.7k_B \end{aligned}$$

Let N and n represent the total number of atoms and number of surface atoms, respectively, and the HFE of one part would be

$$F_M = N E_p^M + (N - n)(E_{\text{vib}} - T S_{\text{vib}}) + n(E_{\text{vib}}^s - T S_{\text{vib}}^s)$$

We suppose the interface, two atomic layers composed of 50% A and 50% B atoms, could be regarded as an amorphous state. We also assume that the enthalpy of phase transformation from the crystalline state to amorphous state is one-half of that of fusion (ΔH_m). Thus, the interface energy can be written as²²

$$\sigma = \left(\frac{N_0}{V}\right)^{2/3} \frac{\Delta H_m}{N_0}$$

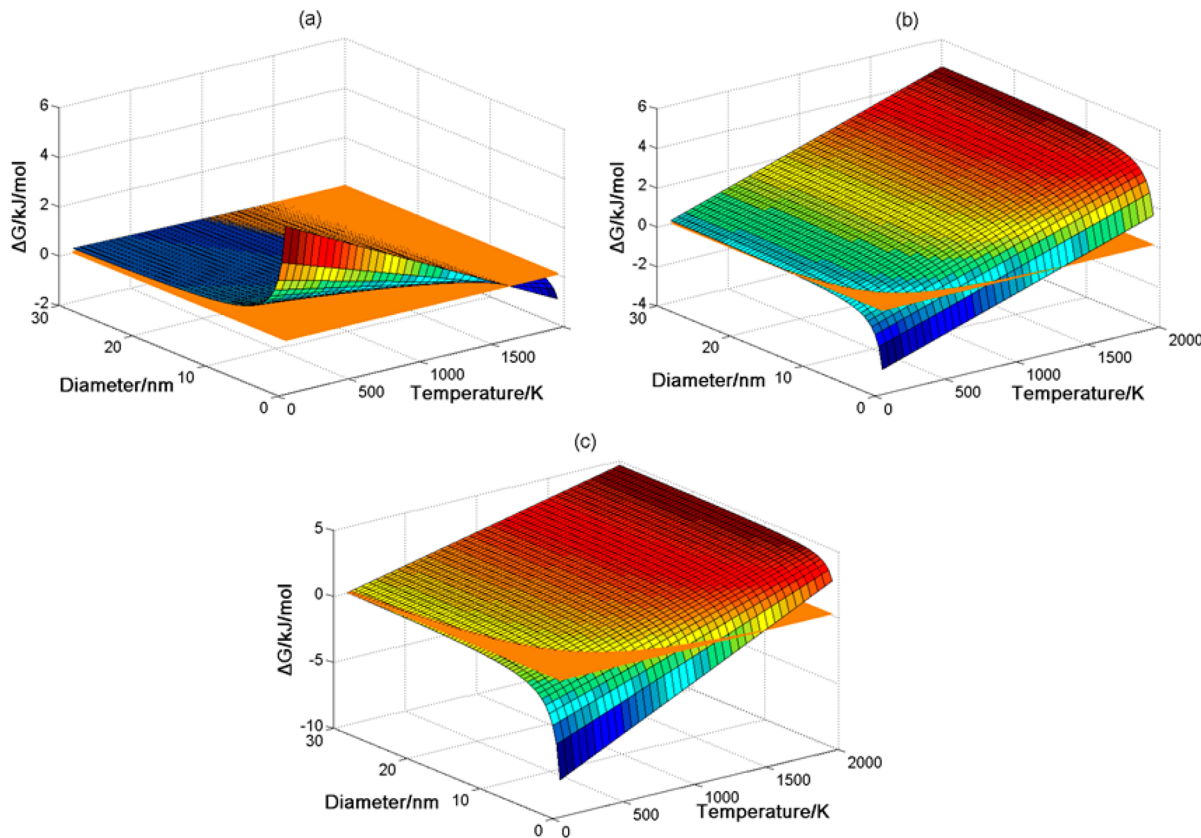


Figure 3. Gibbs free energy difference between (a) Janus and core–shell structure, (b) Janus and alloyed structure, and (c) core–shell and alloyed structure of $\text{Ag}_{0.5}\text{Cu}_{0.5}$ NPs. The brown plane denotes $\Delta G = 0$. $E_{\text{Cu}} = -336 \text{ kJ/mol}$, $E_{\text{Ag}} = -284 \text{ kJ/mol}$, $V_{\text{Cu}} = 7.11 \text{ cm}^3$, $V_{\text{Ag}} = 10.27 \text{ cm}^3$,²³ $\Delta H_m^{\text{Cu}} = -13.1 \text{ kJ/mol}$, $\Delta H_m^{\text{Ag}} = -11.3 \text{ kJ/mol}$.²⁴ The values of surface energy are from ref 13.

where N_0 denotes the Avogadro constant, V is the mean molar volume, $V = ((V_A + V_B)/2)$. $\Delta H_m = ((\Delta H_m^A + \Delta H_m^B)/2)$, where ΔH_m^A and ΔH_m^B are the enthalpy of fusion of A atoms and B atoms, respectively. The unit of σ is J/m^2 . Thus $E_{\text{int}} = \sigma \cdot A_{\text{int}}$ where A_{int} is the area of the interface.

To compare the A–B Janus structure with the A@B core–shell structure (A@B refers to core @ shell), we need to introduce two parameters: volume ratio y , which is the volume percent of A; length ratio z , which is the ratio of the height of spherical cap and the diameter of Janus particle. Therefore, there is a mathematical relationship between y and z :

$$H = zD \quad (0 \leq z \leq 1)$$

$$V_A^J = \pi \cdot D^3 z^2 (3 - 2z) / 6$$

$$A_{\text{int}}^J = \pi \cdot D^2 z (1 - z)$$

$$A_{\text{int}}^{\text{CS}} = \pi \cdot D^2 y^{2/3}$$

$$y = V_A^J / V_{\text{total}} = z^2 (3 - 2z)$$

where J and CS refer to the Janus and core–shell structures, respectively.

The HFE F_M can be rewritten as

$$\begin{aligned} F_M &= NE_p^M + N(E_{\text{vib}} - TS_{\text{vib}}) \\ &\quad + n[(E_{\text{vib}}^s - E_{\text{vib}}) - T(S_{\text{vib}}^s - S_{\text{vib}})] \\ &= NE_p^M + N(E_{\text{vib}} - TS_{\text{vib}}) + n[E_{\text{vib}} - 2.7k_B T] \\ &= NE_p^M + N \left[3k_B \ln(1 - e^{-\Theta/T}) - k_B TB \left(\frac{\Theta}{T} \right) \right] \\ &\quad + n \left[3k_B TB \left(\frac{\Theta}{T} \right) - 2.7k_B T \right] \end{aligned}$$

By replacing N by the Avogadro constant (N_0), the HFE per mole F_M becomes

$$\begin{aligned} F_M &= E + 3RT \ln(1 - e^{-\Theta/T}) - RTB \left(\frac{\Theta}{T} \right) \\ &\quad + \frac{n}{N} \left[3RTB \left(\frac{\Theta}{T} \right) - 2.7RT \right] \end{aligned} \quad (3)$$

where E is the cohesive energy per mole of NPs, and $R = k_B N_0$ is the gas constant.

For A atoms of Janus NPs, $n/N = 4zd_A/yD$, and B atoms of Janus NPs, $n/N = 4(1-z)d_B/(1-y)D$; for A atoms of core–shell NPs, $n/N = 0$, and B atoms of core–shell NPs, $n/N = 4d_B/(1-x)D$.

Comparing Janus and core–shell NPs, the HFE of alloyed ones should consider the configuration entropy. The entropy is defined as $S = k_B \ln W$ according to the Boltzmann equation, where W is the number of arrangements of atoms. For bimetallic alloy structure, $W = N!/(N_A!N_B!)$. So we get the configuration entropy formula:

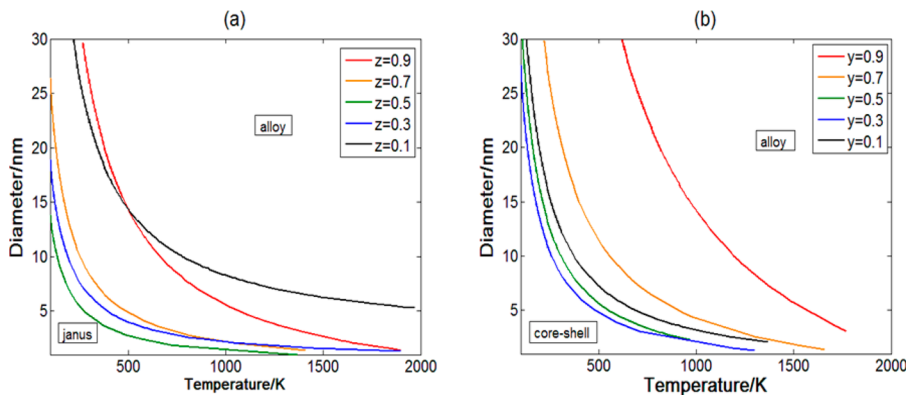


Figure 4. Comparison of two structures of Ag–Cu NPs varying with size D and temperature T at five different Cu atom fractions: (a) Janus and alloyed ones, (b) core–shell and alloyed ones. Upon the critical line, the GFE of alloyed NPs is lower, and the alloyed structure is more stable. Below the critical line, the GFE of Janus (a) or core–shell (b) NPs is lower, and the Janus or core–shell structure is more stable.

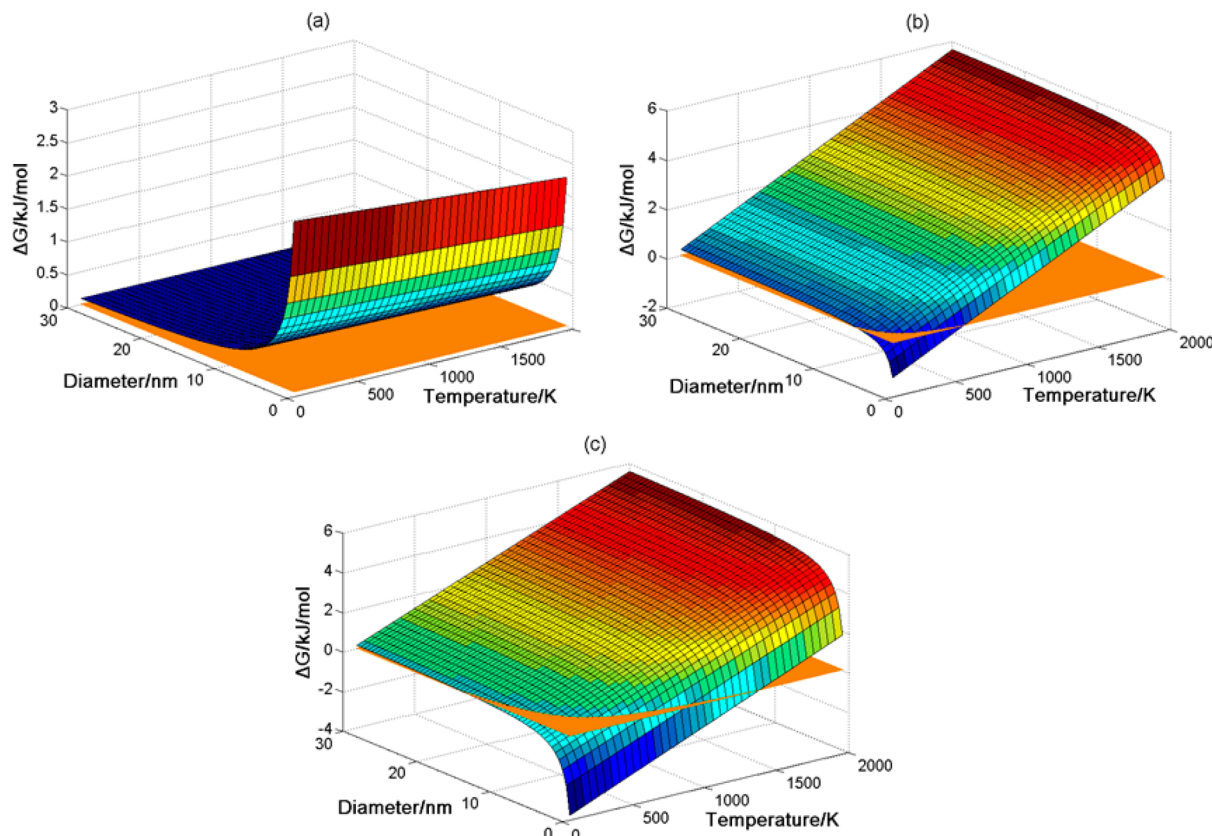


Figure 5. Gibbs free energy difference between different structures of $\text{Ag}_{0.5}\text{Au}_{0.5}$ NPs. (a) Janus and core–shell structure; (b) Janus and alloyed structure; (c) core–shell and alloyed structure. $E_{\text{Au}} = -368 \text{ kJ/mol}$, $V_{\text{Au}} = 10.21 \text{ cm}^3$, $\Delta H_m^{\text{Au}} = -12.5 \text{ kJ/mol}$.²⁴

$$\begin{aligned} S_{\text{conf}} &= k_B \ln \frac{N!}{N_A! N_B!} = k_B N \ln \left(\frac{N_A}{N} \ln \frac{N_A}{N} + \frac{N_B}{N} \ln \frac{N_B}{N} \right) \\ &= k_B N \ln [x \ln x + (1-x) \ln(1-x)] \end{aligned}$$

Replacing N by the N_0 , we get the $S_{\text{conf}} = R \ln [x \ln x + (1-x) \ln(1-x)]$ per mole of alloy NPs.

The relationship between Gibbs free energy (GFE) and HFE is $G = F + PV$, where P is the pressure, and V is the volume. Because the term PV is similar for Janus, core–shell, and alloy NPs in same size and composition, approximately the energy difference between every two structures of HFE and GFE is similar, $\Delta G \approx \Delta F$. Meanwhile, we do not consider the oxidation phenomenon or the influence to free energy by

atmosphere, and thus the present HFE model should be regarded as established in vacuum condition or under the protecting atmosphere such as argon or nitrogen, etc. Here, we have derived the HFE formula of these three structures, by which we can predict the structural stability of bimetallic NPs.

3. RESULTS AND DISCUSSION

There are three independent variables in the equation: NPs' diameter (D), temperature (T), and atom fraction (x , there is a mathematic relationship between parameters x , y , and z). Varying these three variables, we can calculate size-, temperature-, or composition-dependent GFE. Also, the relative

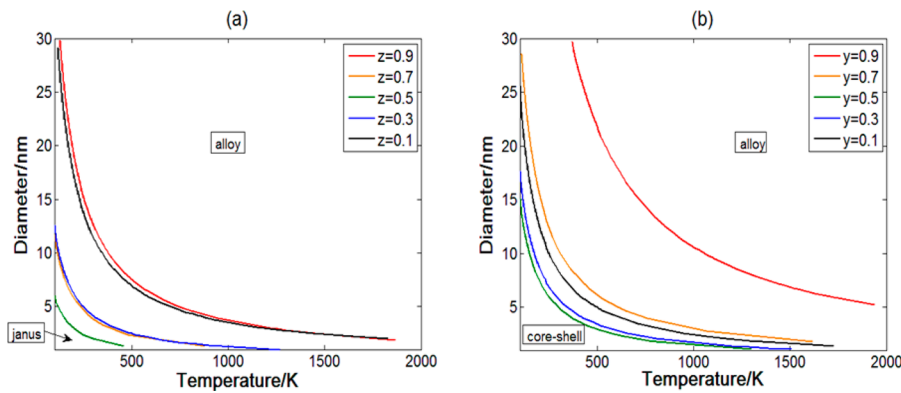


Figure 6. Stable regions of different structures of Ag–Au NPs at different Au atomic fractions. (a) Janus and alloyed; (b) core–shell and alloyed.

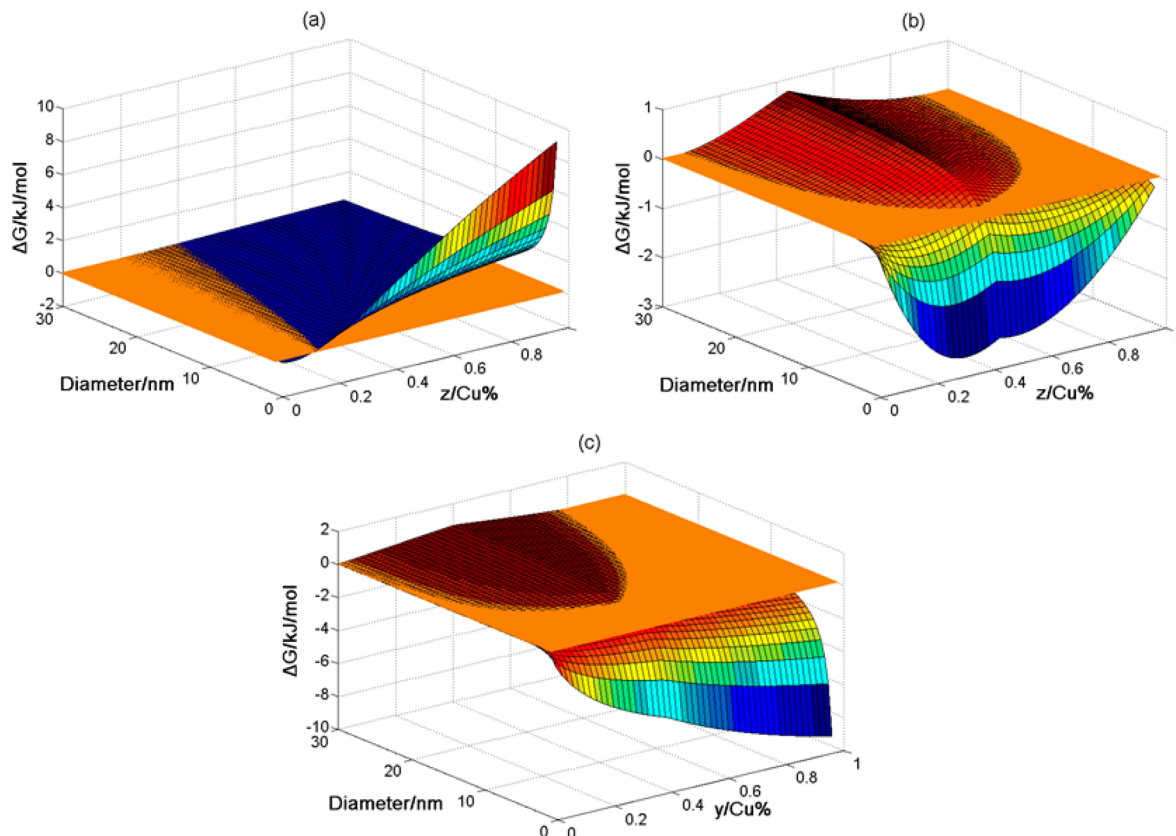


Figure 7. Gibbs free energy difference between different structures of Ag–Cu NPs at ambient temperature. (a) Janus and core–shell; (b) Janus and alloyed; (c) core–shell and alloyed.

structural stability can be obtained by comparing the energies of Janus, core–shell, and alloyed structures.

In the present work, the more negative is the free energy, the more stable is the structure. As we know, the surface energy of Ag is obviously less than that of Cu. So the Cu atom will gather in the interior, and Ag will cover the surface in the core–shell structure. Figure 3 shows the GFE difference ΔG of $\text{Ag}_{0.5}\text{Cu}_{0.5}$ between any two of these structures. The region above the $\Delta G = 0$ plane indicates that the latter one is more stable. In Figure 3a, it can be seen that the critical line almost plumbs to the axis of temperature. At majority temperature range (below about 1500 K), the cured surface lies above the $\Delta G = 0$ plane, which means the core–shell structure is more stable than the Janus one. At large size range, the difference of free energy is comparatively small, and ΔG steeply increases with the

decrease of the size, because the size effect of NPs at small size range is more obvious. It can be inferred that the factors of small size and low temperature benefit core–shell structure. Figure 3b and c structures are similar. At small size and low temperature range, the core–shell or Janus structure is more stable than the alloyed one, and the size and temperature ranges of stable core–shell or Janus NPs are much smaller than those of alloyed ones. From Figure 3, we can find that the Janus structure is more unstable than the core–shell one at low temperature and more unstable than the alloyed one at high temperature. According to our calculation, there is no Janus structure for $\text{Ag}_{0.5}\text{Cu}_{0.5}$ NPs.

Figure 3 shows the case with Cu atom fraction $x = 0.5$. Figure 4 shows the relationship between critical size D and the temperature at different Cu atom fractions (z of Janus in Figure

4a and y of core–shell in Figure 4b). No matter how large the Cu atom fraction is, the critical size D decreases with the increase of temperature. In Figure 4a, the lines of $z = 0.1$ and $z = 0.9$ locate at a similar location, as do the lines of $z = 0.3$ and $z = 0.7$. With the increase of parameter z , the interface area of the Janus structure first expands, becomes the largest at $z = 0.5$, and then shrinks. The interface energy follows the same tendency, which produces the free energy difference between the Janus and alloyed structures. Meanwhile, we find the largest stable region of Janus is at $z = 0.1$ or $z = 0.9$ and the smallest is at $z = 0.5$. Thus, the factor of $z = 0.1$ and $z = 0.9$ contributes much to the Janus structure, and the factor of $z = 0.5$ does the same to the alloyed structure. It is well understood that, when the composition of Cu or Ag atoms is less than that of the other element, Cu or Ag atoms are easy to gather at the surface, forming the Janus structure. By comparison with the Janus structure, the interface area of core–shell increases monotonously with the increase of y . Yet Figure 4b shows the minimum value of atom fraction is $y = 0.3$. This is due to the fact that when the number of Cu or Ag atoms decreases, the configuration entropy will diminish, and consequently alloyed structure will become unstable. Thus, it can be concluded that the factor of $y = 0.9$ is beneficial to the core–shell structure, while the factor of $y = 0.3$ is beneficial to the alloyed structure.

In Figure 5a, it can be found that no matter what size and temperature, $\text{Ag}_{0.5}\text{Au}_{0.5}$ core–shell NPs are more stable than Janus NPs of the same composition. Because the interface energy of Ag–Au is relatively small ($\sigma_{\text{Ag}-\text{Au}} = -0.149 \text{ J/m}^2$), the free energy difference of interior NPs between Au@Ag and Janus is small too. The surface energy of Au is larger than that of Ag, and Au@Ag NPs are covered by Ag atoms, but Janus NPs are covered by 50% Ag atoms and 50% Au atoms. Thus, the free energy of Au@Ag NPs is lower than that of Janus NPs, and the Au@Ag core–shell structure is more stable. Figure 5b and c shows that the stable region of Janus or core–shell is nearly zero, for the interface energy of Ag–Au is small as compared to that of Ag–Cu systems.

In Figure 6a, it is interesting to find out that the critical lines of $z = 0.1$ and $z = 0.9$, $z = 0.3$, and $z = 0.7$ are almost completely overlapped. First, the area of interface at $z = 0.1$ equals that at $z = 0.9$, indicating that their interface energies are equal too. Next, their configuration entropies are almost equivalent. Although the Ag–Au NPs with different atom fractions $z = 0.1$ and $z = 0.9$ have different cohesive energies, the difference is relatively small by comparing the interface energies with configuration entropies. Thus, the critical lines of $z = 0.1$ and $z = 0.9$ are nearly overlapped, as are the lines of $z = 0.3$ and $z = 0.7$.

Bimetallic nanoparticles can be generated in a variety of ways, such as molecular beams, chemical reduction, thermal decomposition, ion implantation, electrochemical synthesis, etc.¹ The general experiment temperature is around 100 °C, even at ambient temperature. Even if there is a subsequent annealing or tempering treatment, the annealing or tempering temperature is highest at about 500 °C.⁴ Thus, it is meaningful to discuss the relationship between critical size D and the atom fraction at a fixed temperature.

In Figure 7a, one can find that, at ambient temperature, the curved surface of free energy difference between Janus and Cu@Ag core–shell NPs is above the $\Delta G = 0$ plane at the region of $z > 0.1$. The critical line is almost parallel to the axis of diameter. This is because the interface area of core–shell is larger than that of Janus when $z > 0.1$; the interface area

difference between Janus and core–shell structures is shown in Figure 8. Besides, the surface energy of core–shell is lower than that of Janus ($E_{\text{Ag}}^s = 0.553 \text{ eV/atom}$, $E_{\text{Cu}}^s = 0.707 \text{ eV/atom}$).

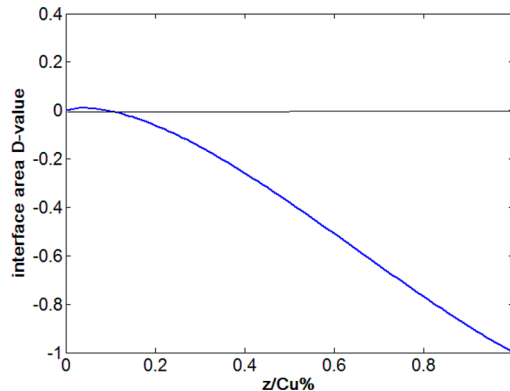


Figure 8. Relationship of the interface area between Janus and core–shell structure with the core atom fraction z . Under the zero line, the core–shell interface area is larger.

Afterward, we calculate the planar structure transformation cases at 400 and 800 K. It can be seen that temperature does not affect the shape of the critical lines, but rather the “height” and radian of the critical lines. The critical size D at 400 K is larger than that at 800 K, and the slope of the critical line at 400 K is greater than that at 800 K as well, which means that the critical size changes more intensely at low temperature. Briefly, low temperature is more beneficial to the phase segregated structure for AgCu NPs. High temperature makes the configuration entropy rise, and then the free energy of alloyed NPs is reduced. Furthermore, the high temperature does help the diffusion of atoms and remit the interior strain by the size mismatch of Ag–Cu NPs. Figure 9 shows that the critical lines of free energy between Janus and alloyed, core–shell, and alloyed have an analogous parabola. When the fraction of Cu atoms is too small (less than about 30%), or too large (greater than about 70%), the critical diameter D is large. Yet when the Cu atom fraction is in the range from 35% to 60%, the critical diameter D is comparative small. It is due to the fact that the configuration entropy of alloyed NPs will trail off as the amount of Ag or Cu atom is small, leading to the free energy of Cu–Ag alloyed NPs to increase, and, as a result, the critical line shows a parabola character. Meanwhile, due to the symmetrical change of interface area of Janus NPs, the critical line of Figure 7b possesses a symmetry axis of roughly $z = 0.5$, as does the core–shell NPs in Figure 7c.

All we discussed above is the comparison of two structures’ stability. If we compare all three structures, we can get the size–composition phase diagram of all three structures, exactly as Figure 10 shows. Similar to Figure 9, the red line denotes the situation $T = 800 \text{ K}$, and the blue line denotes $T = 400 \text{ K}$. It can be seen that the phase diagram is divided into three sections: Janus region, core–shell region, and alloyed region. The alloyed structure lies on the top of the diagram, the region of large size NPs accordingly, the Janus structure lies on the region of small size and large Ag atoms (shell atoms) fraction, and the core–shell structure is located at the region of small size and large Cu atoms (core atoms) fraction. With the increase of temperature, the triphase coordinate moves to low right (from (0.152, 10.76) to (0.230, 3.70)). Above all, the high temperature enlarges the area of alloyed NPs in the phase diagram, which means high

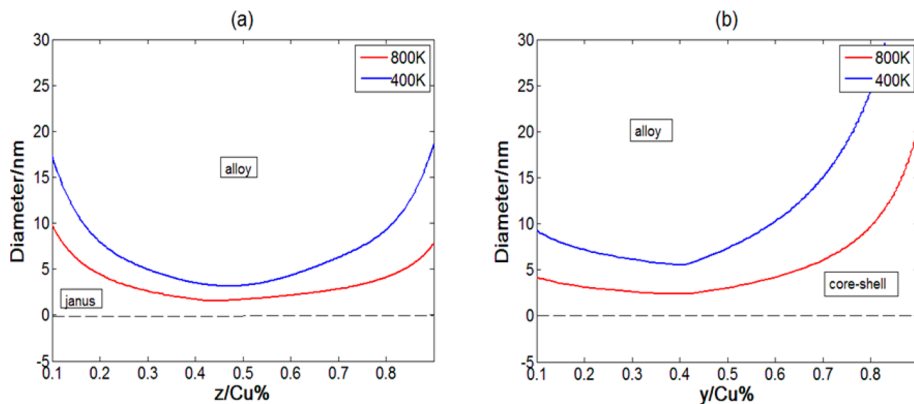


Figure 9. Critical size region for stable structures of Ag–Cu NPs varying with Cu atom fraction at two different temperature. (a) Janus and alloyed; (b) core–shell and alloyed.

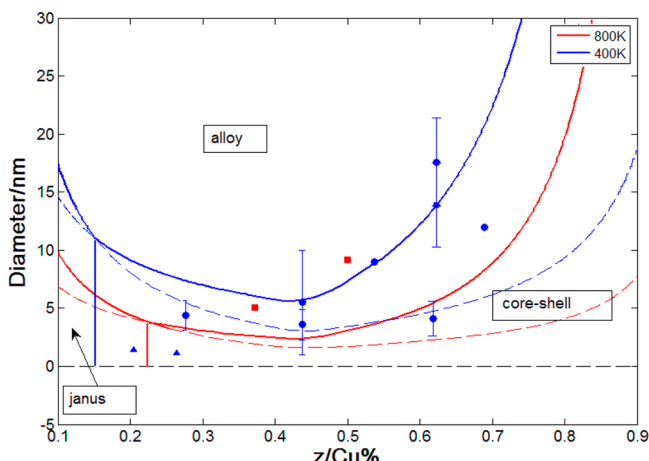


Figure 10. Phase diagram of Ag–Cu NPs ($T = 400$ K and $T = 800$ K) with the variation of particle size and Cu atom fraction. The blue symbols denote the experiment or simulation temperature is close to 400 K; red symbols denote the temperature is closer to 800 K. The referred data are from ▲^{27,28} for Ag–Cu Janus or quasi-Janus NPs, ●^{4,26,29–31} for Cu@Ag NPs, and ■^{33,34} for Ag–Cu alloy NPs.

temperature does help get to alloyed structure and low temperature is conducive to phase segregated structure. If we only consider the phase segregated structure, we can find out that the high temperature phase line moves to the right. For small NPs, the surface to volume ratio increases suddenly and the surface energy will become dominant; thus the Ag atoms have a strong tendency to surface segregation. High temperature will enlarge the energy of alloyed NPs (provided by configuration entropy), and thus the size effect on smaller NPs will be obvious. On the contrary, at high temperature, the fewer Ag or Cu atoms lead to a small configuration entropy, and thus the size effect on NPs may be obvious too. Dotted lines denote the critical lines of metastable state. In the region of core–shell, the Janus is the second stable structure under the dotted line, while between the solid and dotted lines the alloyed structure is second stable. This metastable phase region could help us study the trend of the transformation between different structures. Deng²⁵ pointed out that the surface segregation of NPs will be more obvious as the particle size decreases. Delogu et al.²⁶ calculated the free energy difference between Janus and core–shell, alloyed structures of $\text{Ag}_{50}\text{Cu}_{50}$ NPs using molecular dynamics simulations. They found that the Janus is always the most stable structure at size range from 1 to 10 nm, but the free

energy difference between Janus and core–shell structure is very small. However, they were not sure whether the surface of Cu is covered by a layer of Ag atoms or not. Considering the fact that the surface energy of Ag is lower than that of Cu, we regard it as quasi-Janus or core–shell structure. According to our prediction, for $\text{Ag}_{50}\text{Cu}_{50}$ NPs, core–shell is the most stable structure when the particle size is smaller than ~ 7 nm. As the particle size becomes smaller than ~ 4 nm, the Janus structure may be the second stable phase. Thus, $\text{Ag}_{50}\text{Cu}_{50}$ NPs have a tendency to transform from core–shell to Janus when particle size is small, which could explain the situation of quasi-Janus NPs. Laasonen et al.²⁷ predicted the motifs of Ag–Cu NPs with density functional theory (DFT) calculation. They predicted that $\text{Ag}_{414}\text{Cu}_{147}$ NPs (the particle size is 1.16 nm, and the Cu atoms volume ratio is 19.63%) are more likely to display the off-centered core–shell motif rather than the centered motif. Besides, according to Bochicchio's studies,¹² strain causes a different influence to icosahedral and decahedral or fcc Ag–Cu NPs. For Ag-rich fcc crystalline and decahedral motifs, off-centered core–shell structure is the lowest-energy one. Yet for icosahedral motif, centered core–shell is stable when the Cu core is not large enough, and once the Cu core exceeds the critical size, the morphological instability will drive the Cu core to the asymmetric configuration. The strain relaxation is the physical factor responding for these conditions. So we can consider that, in most cases, off-centered Cu core does a better strain release if the core is sufficiently large. These agree with the prediction of our phase diagram, while the $\text{Ag}_{414}\text{Cu}_{147}$ NPs lie in the core–shell region and close to the Janus one. Atanasov et al.²⁸ calculated the motifs of Ag–Cu NPs, and they found the quasi-Janus motif with size of 1000 atoms and 15 at. % Cu atoms, corresponding to a Cu volume fraction of 10.83%. Muzikansky et al.²⁹ synthesized Cu@Ag NPs at three different temperatures, and then did an aging treatment. They fabricated Cu@Ag NPs with diameters of 13.9 ± 3.6 and 17.6 ± 3.8 nm at temperature $T = 120$ °C; the atomic ratio is 3.1:1 (corresponding to Cu atoms volume fraction of 68.08%), before and after 12 months aging, respectively. Langlois et al.⁴ synthesized Cu@Ag NPs by a physical route with the substrate temperature of 270 °C. One sample of Cu@Ag NPs' mean diameter is 12 nm, and the Ag shell thickness is 1 nm. By comparison with the simulation results, they came to the conclusion that when the concentration of core atoms is relatively few, the energy difference of centered and off-centered positions will increase quickly. This conforms to our standpoint. Cazayous et al.³⁰ measured Cu@Ag NPs by

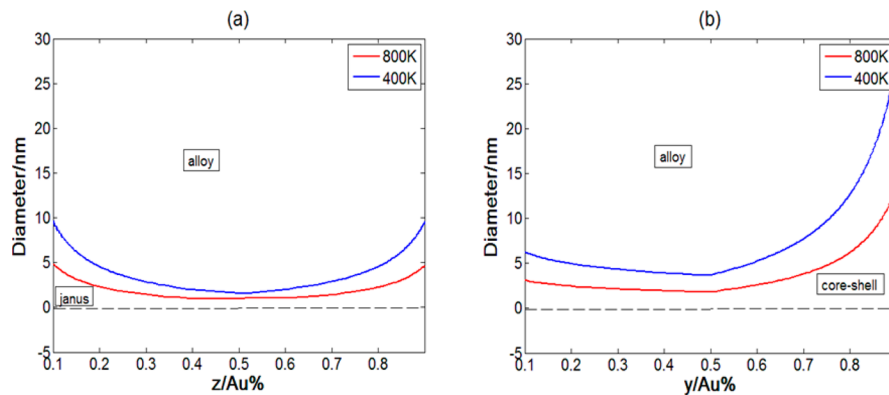


Figure 11. Critical size of two structures of Ag–Au NPs varying with Au atom fraction at two different temperatures. (a) Janus and alloyed; (b) core–shell and alloyed.

confocal micro-Raman spectroscopy. For the Cu@Ag size of 9 nm, the Ag shell thickness is 1.6 nm. These NPs just right lie on the phase line between core–shell and alloyed structures. Itakura et al.³¹ prepared Cu₂₅Ag₇₅, Cu₅₀Ag₅₀, and Cu₇₅Ag₂₅ core–shell NPs by UV irradiation with the sizes of 4.4 ± 1.27, 3.6 ± 1.31, and 4.1 ± 1.46 nm, respectively. Moreover, the Cu₇₅Ag₂₅ core–shell NPs could possibly form an anti-Mackay and chiral Ag shell. Bochicchio and Ferrando³² reported that the tendency to surface segregation of Ag atoms and the weak tendency to intermixing of Ag–Cu are factors to form the core–shell structure, and the size mismatch of Ag and Cu atoms may generate the anti-Mackay and chiral icosahedral shell. We think this condition will take place only when the NPs size is relatively small. Tabrizi et al.³³ researched the generation of Ag–Cu mixed metallic NPs by spark discharge. They got Ag–Cu nanoalloy with a size of about 5 nm, which is 28 wt % Cu and 72 wt % Ag (corresponding to a Cu volume fraction of 31.10%). Ceylan et al.³⁴ prepared the Ag–Cu alloy NPs by inert gas condensation process, with the volume ratio of 1:1 and average size 9.1 nm, at the temperature range between 800 and 1400 °C. These studies of Ag–Cu NPs agree well with the predictions of our phase diagram.

As compared to the Ag–Cu NPs, the Ag–Au NPs have a tendency to form alloyed structure, which agrees with our calculation and Ag–Au phase diagram. From Figure 11, we can find that the area of alloyed region is larger than that of Ag–Cu NPs. Actually, it is the consequence of two reasons. The first one is the miscibility of Ag and Au atoms in bulk state. They have similar atom radius and the same crystal structure, meaning that the mixed Ag–Au NPs do not produce too much inter strain. Their locations in periodic table of elements are neighboring; that is, their chemical properties are closed, such as the strength of binding to ligands, the specific electronic effects, and charge transfer between heterogeneous atoms. The second reason is that formation enthalpy of Ag–Au is negative. In Figure 11a, the critical size of the transform between alloyed and Janus structure is very low (about 3 nm) at the scope of $z = 0.3$ to $z = 0.7$. Figure 11b shows that the critical size between alloyed and core–shell structures is not large until the Au fraction is larger than about 65%. However, for both core–shell or Janus NPs, the lowest critical size occurred at about 50% Au atom fraction, corresponding to the most favored structure of alloyed NPs. Identical to the case of the Ag–Cu, the high temperature is beneficial to the formation of Ag–Au alloyed structure. Moreover, Ag@Au NPs have been studied by some research. Chen et al.³⁵ studied the 13 atoms Ag–Au

nanocluster by semiempirical potentials and DFT calculations. The result showed that the Au-surface-segregated cluster is most stable, which is enhanced by directional charge transfer. Cerbelaud et al.³⁶ reported that, in a small cluster, Au atoms are preferred to segregate to the surface, which is related to the charge transfer between Ag and Au. Because electronegativity and hardness depended on the coordination of Ag and Au atoms, Ag will get a positive charge and Au will lose a positive charge. However, the phenomenon of Au enrichment of the NPs surface occurs generally in a small size, and the influence of the charge transfer will trail off when the particle size is about 1 nm.

Combining Figure 11a and b mentioned above, we can get the size- and composition-dependent phase diagram of Ag–Au NPs as in Figure 12. It is interesting to notice that, no matter

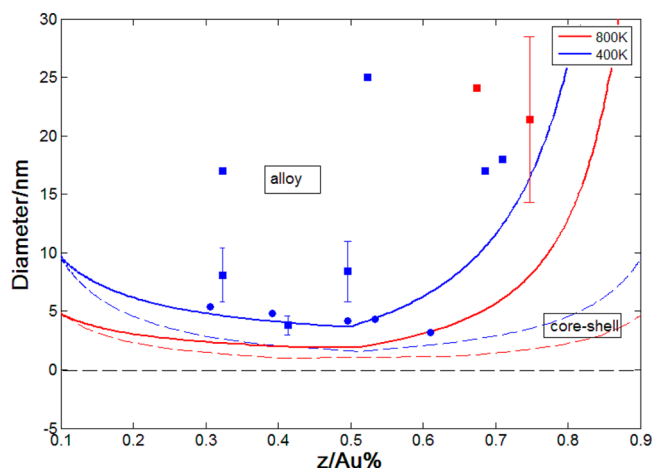


Figure 12. Phase diagram of Ag–Au NPs ($T = 400\text{ K}$ and $T = 800\text{ K}$) with the variation of particle size and Au atoms fraction. The blue symbols denote the experiment or simulation temperature is close to 400 K; red symbols denote the temperature is closer to 800 K. The referred data are from ●^{41,42} for Au@Ag NPs, and ■^{37–40} for Ag–Au alloy NPs.

what the temperature is, two critical size lines (the solid lines and dotted lines) are intersected at about Au fraction $z = 0.1$; that is, the Janus structure will no longer appear when $z > 0.1$. Yet as long as we study the phase diagram, we can find out that under the dotted lines the Janus is the second stable phase, and among the solid lines and dotted lines, the alloyed is the second stable phase. On the basis of these results, we can study the

particle growth. The more Au atoms there are, the more possible the phase segregated structure is stable. So the large Au atoms fraction is the one of the pledge to form core–shell structure. If we fix the size of Ag–Au NPs, the larger Au core or smaller Ag shell thickness will benefit the core–shell structure. Wang et al.³⁷ prepared the Ag–Au alloy NPs in the hydrothermal reaction at 100 °C, and then reduced at 600 °C. The particles sizes are measured as 21.4 and 24.1 nm by TEM with Au/Ag molar ratio of 5.37 and 3.07, and the corresponding coordinates lie in the alloyed region in Figure 12. It indicates that through thermal treatment of higher temperature (around 800 K), the Ag–Au particles tend to grow larger and mix to form alloyed structure. Shang et al.³⁸ synthesized the Ag–Au alloy NPs by the virtue of polyelectrolyte multilayer (PEM) nanoreactors. They prepared Ag–Au NPs with size of 3.8 ± 0.8 nm and 40 at. % Au, and the reaction temperature $T = 473$ K. According to our predictions, the Ag–Au particles of 3.8 nm will be in alloyed structure at 400 K and in core–shell one at 800 K, which agrees well with the experimental data. Link et al.³⁹ fabricated 17, 25, 17, and 18 nm Ag–Au alloy NPs with the Au mole fractions of 27%, 54%, 77%, and 80%, respectively. The reaction temperature is the boiling point of aqueous solution. Zhang et al.⁴⁰ synthesized various component Ag–Au alloy NPs by using Cacumen platycladi extract at $T = 90$ °C. The NPs with 8.4 ± 2.6 and 8.1 ± 2.3 nm, 1/1 and 1/3 Au atoms ratio, lie on the alloy region. Li et al.⁴¹ synthesized Au@Ag NPs by an inverse micelle method. They obtained 3.2, 4.2, 4.8, and 5.4 nm as the Au:Ag molar ratio was 2:1, 1:1, 1:1.9, and 1:3.4. The four coordinate points are next to the phase line between the alloyed and core–shell structures. Shinata et al.⁴² prepared the Au@Ag NPs by radiolytic wet techniques at ambient temperature; meanwhile, they simulated the Ag–Au NPs with molecular dynamics simulation. They concluded that the Au@Ag NPs with the size of 4.3 nm and Ag/Au atom ratio of 0.8 are stable and lie on the boundary of the core–shell region of our predicted phase diagram. From the experimental data above, it can be seen that most of the data fit our phase diagram, and we can confirm that our phase diagram could predict Au–Ag NPs’ structure qualitatively.

Combining Figure 10, Figure 12, and our HFE formula, we can do some predictions, such as formulating the annealing temperature for alloying of NPs. Hirai et al.⁴³ synthesized Ag–Cu nanoalloy with Cu content of 14 at. % by pulsed laser deposition (PLD) method, and then an annealing treatment. With increasing annealing temperature from 300 to 548 K, the diameter of NPs varies from 15.2 ± 4.0 to 24.9 ± 14.0 nm; among these, the smallest size is 10.9 nm. According to Figures 10 and 4, for the NPs of about 10 nm, the annealing temperature for alloying is at least 400 K, which agrees with the experimental results.

4. CONCLUSIONS

In our work, the GFE formula for bimetallic NPs with different structures has been derived by combining the bond-energy model and Debye theory, while there are four variables: size, temperature, atom fraction, and three varieties of particle structure. To our best knowledge, we have not found other works considering all four factors affecting phase stability at the same time. Using the GFE formula, we plot the size- and composition-dependent phase diagram. For Ag–Cu NPs, the immiscibility in bulk state, the strong difference of their surface energy, and the positive formation enthalpy lead the Ag–Cu

NPs to be more possible to form phase segregated structure. All of these have been reflected in our phase diagram: for small size particles (less than about 5 nm) and small element fractions, the phase segregated (Janus or core–shell) structure is most stable. Generally, when the core size of core–shell NPs diminishes, the core position will change from centered to off-centered until only a thin shell atom layer covers the core, that is, forming the Janus structure. Meanwhile, the surface-to-volume ratio will trail off when particles become large, indicating the surface effect gives less contribution to NPs’ free energy, and the alloyed structure will be favored. For Ag–Au NPs, they totally differ from Ag–Cu NPs, regarding the miscibility in bulk state, the relatively small difference of their surface energy, and the negative formation enthalpy. Thus, in the Ag–Au phase diagram, the stable region of alloyed structure is larger, and there is no Janus structure. In short, the present work can be widely used in designing and synthesizing new bimetallic NPs with different structures.

■ AUTHOR INFORMATION

Corresponding Author

*E-mail: qiwh216@csu.edu.cn.

Notes

The authors declare no competing financial interest.

■ ACKNOWLEDGMENTS

This work was supported by the National Nature Science Foundation of China (Grant nos. 21373273, 51474239), the Hunan Provincial Natural Science Foundation of China (Grant no. 13JJ1002), and the Shenghua Scholar Program of Central South University.

■ REFERENCES

- (1) Ferrando, R.; Jellinek, J.; Johnston, R. L. Nanoalloys: From Theory to Applications of Alloy Clusters and Nanoparticles. *Chem. Rev.* **2008**, *108*, 845–910.
- (2) Walther, A.; Muller, A. H. E. Janus Particles: Synthesis, Self-Assembly, Physical Properties, and Applications. *Chem. Rev.* **2013**, *113*, 5194–5261.
- (3) Paz-Borbon, L. O.; Gupta, A.; Johnston, R. L. Dependence of the Structures and Chemical Ordering of Pd–Pt Nanoalloys on Potential Parameters. *J. Mater. Chem.* **2008**, *18*, 4154–4164.
- (4) Langlois, C.; Li, Z. L.; Yuan, J.; Alloyeau, D.; Nelayah, J.; Bochicchio, D.; Ferrando, R.; Ricolleau, C. Transition from Core–Shell to Janus Chemical Configuration for Bimetallic Nanoparticles. *Nanoscale* **2012**, *4*, 3381–3388.
- (5) Logsdail, A. J.; Johnston, R. L. Predicting the Optical Properties of Core–Shell and Janus Segregated Au–M Nanoparticles (M = Ag, Pd). *J. Phys. Chem. C* **2012**, *116*, 23616–23628.
- (6) Parsina, I.; Baletto, F. Tailoring the Structural Motif of AgCo Nanoalloys: Core/Shell versus Janus-like. *J. Phys. Chem. C* **2010**, *114*, 1504–1511.
- (7) Song, Y.; Liu, K.; Chen, S. AgAu Bimetallic Janus Nanoparticles and Their Electrocatalytic Activity for Oxygen Reduction in Alkaline Media. *Langmuir* **2012**, *28*, 17143–17152.
- (8) Xu, Y. H.; Wang, J. P. Direct Gas-Phase Synthesis of Heterostructured Nanoparticles through Phase Separation and Surface Segregation. *Adv. Mater.* **2008**, *20*, 994–999.
- (9) Xiong, S. Y.; Qi, W. H.; Huang, B. Y.; Wang, M. P.; Li, Y. J. Size and Shape Dependent Gibbs Free Energy and Phase Stability of Titanium and Zirconium Nanoparticles. *Mater. Chem. Phys.* **2010**, *120*, 446–451.
- (10) Xiong, S. Y.; Qi, W. H.; Huang, B. Y.; Wang, M. P.; Wei, L. Y. Gibbs Free Energy and Size–Temperature Phase Diagram of Hafnium Nanoparticles. *J. Phys. Chem. C* **2011**, *115*, 10365–10369.

- (11) Li, Y.; Qi, W. H.; Huang, B. Y.; Wang, M. P. Modeling the Size- and Shape-Dependent Surface Order–Disorder Transition of $\text{Fe}_{0.5}\text{Pt}_{0.5}$ Nanoparticles. *J. Phys. Chem. C* **2012**, *116*, 26013–26018.
- (12) Bochicchio, D.; Ferrando, R. Morphological Instability of Core-Shell Metallic Nanoparticles. *Phys. Rev. B* **2013**, *87*, 165435–165447.
- (13) Brandes, E. A. *Smithells Metals Reference Book*, 7th ed.; Bath Press: Great Britain, 1992.
- (14) Qi, W. H.; Wang, M. P. Size and Shape Dependent Melting Temperature of Metallic Nanoparticles. *Mater. Chem. Phys.* **2004**, *88*, 280–284.
- (15) Qi, W. H.; Wang, M. P.; Liu, Q. H. Shape Factor of Nonspherical Nanoparticles. *J. Mater. Sci.* **2005**, *40*, 2737–2739.
- (16) Landau, L. A.; Lifshitz, E. M. *Statistical Physics*; Pergamon Press: Oxford, UK, 1958.
- (17) Ostanin, S. A.; Trubitsin, V. Y. A Simple Model for Calculating the P–T phase diagram of Ti. *J. Phys.: Condens. Matter* **1997**, *9*, L491–L496.
- (18) Chen, Q.; Sundman, B. Calculation of Debye Temperature for Crystalline Structures—A Case Study on Ti, Zr, and Hf. *Acta Mater.* **2001**, *49*, 947–947.
- (19) Chen, Z. P.; Wen, Z.; Jiang, Q. Phase Stabilities of fcc Ti Nanocrystals. *Solid State Commun.* **2004**, *132*, 747–750.
- (20) Sun, C. Q. Size Dependence of Nanostructures: Impact of Bond Order Deficiency. *Prog. Solid State Chem.* **2007**, *35*, 1–159.
- (21) Yang, X. X.; Li, J. W.; Zhou, Z. F.; Wang, Y.; Yang, L. W.; Zheng, W. T.; Sun, C. Q. Raman Spectroscopic Determination of the Length, Strength, Compressibility, Debye Temperature, Elasticity, and Force Constant of the C-C Bond in Graphene. *Nanoscale* **2012**, *4*, 502–510.
- (22) Yasuji, N. *The Microstructure of Thermodynamics*, 1st ed.; The Japan Institute of Metal Press: Japan, 2005.
- (23) Kittel, C. *Introduction to Solid State Physics*, 8th ed.; Wiley: New York, 1967.
- (24) <http://www.webelements.com>.
- (25) Deng, L.; Hu, W. Y.; Deng, H. Q.; Xiao, S. F.; Tang, J. F. Au–Ag Bimetallic Nanoparticles: Surface Segregation and Atomic-Scale Structure. *J. Phys. Chem. C* **2011**, *115*, 11355–11363.
- (26) Delogu, F. Free Energy Differences between Ag–Cu Nanophases with Different Chemical Order. *J. Phys. Chem. C* **2010**, *114*, 19946–19951.
- (27) Lassonen, K.; Panizon, E.; Bochicchio, D.; Ferrando, R. Competition between Icosahedral Motifs in AgCu, AgNi and AgCo Nanoalloys: a Combined Atomistic-DFT Study. *J. Phys. Chem. C* **2013**, *117*, 26405–26413.
- (28) Atanasov, I.; Ferrando, R.; Johnston, R. L. Structure and Solid Solution Properties of Cu–Ag Nanoalloys. *J. Phys.: Condens. Matter* **2014**, *26*, 275301–275308.
- (29) Muzikansky, A.; Nanikashvili, P.; Grinblat, J.; Zitoun, D. Ag Dewetting in Cu@Ag Monodisperse Core–Shell Nanoparticles. *J. Phys. Chem. C* **2013**, *117*, 3093–3100.
- (30) Cazayous, M.; Langlois, C.; Oikawa, T.; Ricolleau, C.; Sacuto, A. Cu–Ag Core–Shell Nanoparticles: A Direct Correlation between micro-Raman and Electron Microscopy. *Phys. Rev. B* **2006**, *73*, 113402–113405.
- (31) Itakura, T.; Torigoe, K.; Esumi, K. Preparation and Characterization of Ultrafine Metal Particles in Ethanol by UV Irradiation Using a Photoinitiator. *Langmuir* **1995**, *11*, 4129–4134.
- (32) Bochicchio, D.; Ferrando, R. Size-Dependent Transition to High-Symmetry Chiral Structures in AgCu, AgCo, AgNi, and AuNi Nanoalloys. *Nano Lett.* **2010**, *10*, 4211–4216.
- (33) Tabrizi, N. S.; Xu, Q.; Pers, N. M. v. d.; Schmidt-Ott, A. Generation of Mixed Metallic Nanoparticles from Immiscible Metals by Spark Discharge. *J. Nanopart. Res.* **2010**, *12*, 247–259.
- (34) Ceylan, A.; Jastrzembski, K.; Shah, S. I. Enhanced Solubility Ag–Cu Nanoparticles and Their Thermal Transport Properties. *Metall. Mater. Trans. A* **2006**, *37A*, 2033–2038.
- (35) Chen, F. Y.; Johnston, R. L. Charge Transfer Driven Surface Segregation of Gold Atoms in 13-Atoms Au–Ag Nanoalloys and Its Relevance to Their Structural, Optical and Electronic Properties. *Acta Mater.* **2008**, *56*, 2374–2380.
- (36) Cerbelaud, M.; Ferrando, R.; Barcaro, G.; Fortunelli, A. Optimization of Chemical Ordering in AgAu nanoalloys. *Phys. Chem. Chem. Phys.* **2011**, *13*, 10232–10240.
- (37) Wang, A. Q.; Liu, J. H.; Lin, S. D.; Lin, T. S.; Mou, C. Y. A Novel Efficient Au–Ag Alloy Catalyst System: Preparation, Activity, and Characterization. *J. Catal.* **2005**, *233*, 186–197.
- (38) Shang, L.; Jin, L. H.; Guo, S. J.; Zhai, J. F.; Dong, S. J. A Facile and Controllable Strategy to Synthesize Au–Ag Alloy Nanoparticles within Polyelectrolyte Multilayer Nanoreactors upon Thermal Reduction. *Langmuir* **2010**, *26*, 6713–6719.
- (39) Link, S.; Wang, Z. L.; El-Sayed, M. A. Alloy Formation of Gold–Silver Nanoparticles and the Dependence of the Plasmon Absorption on Their Composition. *J. Phys. Chem. B* **1999**, *103*, 3529–3533.
- (40) Zhang, G. L.; Du, M. M.; Li, Q. B.; Li, X. L.; Huang, J. L.; Jiang, X. D.; Sun, D. H. Green Synthesis of Au–Ag Alloy Nanoparticles Using Cacumen Platycladi Extract. *RSC Adv.* **2013**, *3*, 1878–1884.
- (41) Li, Z. Y.; Wilcoxon, J. P.; Yin, F.; Chen, Y.; Palmer, R. E.; Johnston, R. L. Structures and Optical Properties of 4–5 nm Bimetallic AgAu Nanoparticles. *Faraday Discuss.* **2008**, *138*, 363–373.
- (42) Shibata, T.; Bunker, B. A.; Zhang, Z. Y.; Meisel, D.; Vardeman, C. F.; Gezelter, J. D. Size-Dependent Spontaneous Alloying of Au–Ag Nanoparticles. *J. Am. Chem. Soc.* **2002**, *124*, 11989–11996.
- (43) Hirai, M.; Kumar, A. Wavelength Tuning of Surface Plasmon Resonance by Annealing Silver–Copper Nanoparticles. *J. Appl. Phys.* **2006**, *100*, 014309–014312.